Construction and Building Materials 248 (2020) 118625

Contents lists available at ScienceDirect

Construction and Building Materials

journal homepage: www.elsevier.com/locate/conbuildmat

Digital image correlation and reliability-based methods for the design and repair of pressure pipes through composite solutions

Roberto García-Martin [a], Jorge López-Rebollo [b,*], Luis Javier Sánchez-Aparicio [c], José G. Fueyo [a], Javier Pisonero [b], Diego González-Aguilera [b]

[a] Department of Mechanical Engineering, University of Salamanca, Higher Polytechnic School of Zamora, Campus Viriato, Avenida Requejo, 33, 49022 Zamora, Spain
[b] Department of Cartographic and Land Engineering. University of Salamanca, Higher Polytechnic School of Ávila, Hornos Caleros, 50, 05003 Ávila, Spain
[c] Department of Construction and Technology in Architecture (DCTA), Polytechnic University of Madrid, Av. Juan de Herrera 4, 28040 Madrid, Spain

HIGHLIGHTS

- The DIC methodology allowed to extract the PDF of the main mechanical properties.
- The use of an adaptative space PCE metamodel has allowed the reduction of the computational time.
- The use of Sobol indices have allowed the evaluation of the input variables in the output response.

ARTICLE INFO

Article history:
Received 13 December 2019
Received in revised form 28 January 2020
Accepted 28 February 2020
Available online 6 March 2020

Keywords:
Digital Image Correlation
Reliability-based methods
Polynomial Chaos Expansion
Carbon fiber
Pressure Pipes

ABSTRACT

This work aims to develop an approach for the reliability-based analysis for the design and repair of pressurized pipes by means of composite solutions. To this end, the approach uses a simulation method to estimate the failure probability of the solution based on the Monte Carlo approach and a Polynomial Chaos Expansion surrogate metamodeling strategy. This combination allows us to reduce the computational time required for evaluating the system's probability of failure as well as extracting the Sobol' indices during the sensitivity analysis stage. The uncertainties related with the composite solution were obtained by means of the Digital Image Correlation approach, allowing us to extract the Probabilistic Distribution Functions (PDF) of its main mechanical parameters. This methodology is validated through the design and repair of a pressurized pipe using a carbon fiber solution and roll wrapping technology. The results show the strong potential of the proposed methodology for the safety evaluation of pressurized composite pipes.

1. Introduction

There are many applications of pressurization based on liquid storing and gas and oil transportation, e.g. underground steel pipelines are one of the most effective and safest systems for oil and gas transportation over a long distance [1,2]. Due to their exposure to environmental agents, metal pipes can corrode, considerably affecting their useful life and thus the economy of the countries [3]. The behaviour of metal pipes is well known, in terms of both mechanical design and lifecycle problems. Furthermore, most of these applications are subject to different regulations and standards, and are frequently revised in the knowledge progress [4].

Step by step, new material solutions have been replacing the traditional steel applications towards composite materials [5]. This is due to their combination of properties providing a high performance index [6–8], and a good long-term performance [9–11]. Therefore, these new materials represent a very interesting solution for high corrosion and mechanical loaded environments, e.g. chemical industry piping. Within this context, the most common material solution is the fiber-reinforced polymer (FRP), mainly by carbon (CFPR) or glass (GFPR) fiber into an epoxy resin matrix [5,8,12–14]. Several techniques could be used for manufacturing FRP pipes, [1,5,9,12,14,15]. Among them, roll wrapping technology is interesting, since it opens up a new field of application: the reparation of steel pipes [5,16–18]. The use of this approach for

* Corresponding author.
E-mail addresses: toles@usal.es (R. García-Martin), jorge_lopez@usal.es (J. López-Rebollo), lj.sanchez@upm.es (L.J. Sánchez-Aparicio), fueyo@usal.es (J.G. Fueyo), j_pisonero@usal.es (J. Pisonero), daguilera@usal.es (D. González-Aguilera).

https://doi.org/10.1016/j.conbuildmat.2020.118625
0950-0618/

Nomenclature

DoE	Design of Experiments	P_f	Probability of failure
E	Young's Modulus	$TSFD$	Tensile Strength Fiber Direction
MIG	Mean Intensity Gradient of the speckle pattern	β	Reliability index
PDF	Probabilistic Distribution Functions	υ	Poisson's ratio

repairing pipes could overcome the main problems of the traditional methods, as well as offering better resisntance and performance [16].

However, these new composite solutions entails difficulties to determine accurately its properties due to the preesnce of heterogeneous properties [19] and their highly directional behaviour [20,21]. Within this context, the contact techniques are not capable of properly capturing the mechanical behaviour of these solutions [22–24]. To overcome this drawback, several full-field optical methods have been developed [25–27]. Among them, Digital Image Correlation (DIC) has become as one of the most promising tools. This method allows us to obtain a full-field of displacements and strains through the use of correlation-based matching procedures and numerical differentiation algorithms [28]. Thanks to this major advantage, DIC has been widely used for the experimental testing of composite solutions under different loading configurations [22,29–34]. Data obtained by this method is commonly used for the evaluation of strain distribution, damage analysis and microstructure observation [22,29,34,35] and, to a lesser extent, as input for probabilistic analysis [36]. This approach, probabilistic analysis, is considered to be the most reliable strategy for numerical simulation of composite solutions [37–39]. In contrast to deterministic methods, the main goal of these approaches is to determine the probability of failure of a mechanical system under the influence of different uncertainties, such as loads or material properties among others [38]. Studies carried out by Rafiee and Ali Torabi [38] and Rafiee et al. [40 39], highlights the relevance of considering these manufacturing uncertainities since it is highly likely that composite prototypes experience faliures bellow the deterministic value. As stated Sriramula and Chryssanthopoulos [21], these uncertainities mght be considered at a constitutent, ply or component level. The estimation of this probability of failure could be carried out by means of approximation methods such as the First (FORM) and Second Order Reliability (SORM) methods or even by means of simulation strategies such as the Monte Carlo Sampling (MCS) method [41]. MCS highlights for its simple and direct implementation [38,39]. However, the cost of this approach increases rapidly when a low probability of failure is required [37], requiring a huge number of simulations and a large computational time [38]. To cope with this lamination, variance reduction techniques and metamodels are commonly used [37,42]. As a result of these techniques, it is possible to construct an equivalent and computationally inexpensive mathematical replica of the system, allowing the carrying out of huge numbers simulations with great accuracy.

As a consequence, this paper therefore aims to progress the effective integration of the DIC approach with the latest advances in probabilistic analysis of engineering solutions. To this end, this approach integrates a surrogate modelling strategy and a reliability analysis with the aim of obtaining the failure probability of a composite solution used for the design and repair of pressurized pipes. In the Methods (Section 2) we describe the composite materials used as well as the experimental and numerical strategies adopted. In Section 3, we show the experimental results obtained by the combination of DIC and the reliability approach in the design and repair of pressurized pipes. Finally, in the Conclusion (Section 4) we summarise the findings and discuss future studies.

2. Materials and methods

2.1. Composite solution evaluated

Compared to other materials or other composites solutions such as GFPR, carbon fiber capabilities exceed those of its competitors. It should be noted that the surface of the carbon fiber is a microcrystalline graphite structure, which entails that the distribution of stresses and the generation and propagation of fissures can be adjustable [43]. In addition, its resistance to high temperatures and corrosion must be considered. All this makes carbon fiber the most suitable material for high-performance pipes [44].

Hence, the material used for testing was a carbon fiber polymer reinforcement CC 200 T-120® with a thickness of 0.32 mm (Table 1), an epoxy resin matrix CR82® and a hardener Biresin CH80-10®. Technical characteristics of epoxy resin and hardener are the same as used by García-Martin et al. [36]. The material has been made from a 200 g Plain where 9 plates of 21 × 29 cm have been obtained. The mix ratio, for a specific amount of 200 g, was 158 g of resin plus 42 g of hardener.

The first layer of reinforcement was placed with proper orientation, then it was impregnated by the resin and catalyst mixture. This process was repeated a total of nine times giving as a result a composite solution made up by nine layers: [±90]9. Each time a layer was added, a light pressure was exerted in order to remove the resin surplus. To obtain the desired thickness of 2 mm [45], the mold was machined with the proper measure. The block was cured in a drying oven for 50 min, at a temperature of 50 °C. Once the material was prepared, the specimens were machined with the proper dimensions (Fig. 1). During this process, computer numerical controlled cutting was used, and programmed according to current regulations specifications [45].

2.2. Mechanical characterization of the composite solution: the 2D digital image correlation method

The composite solution was evaluated by means of tensile tests according to guideline ISO 527 [45]. The electromechanical tensile machine Servosis ME-405/50/5 technical specifications are shown in Table 2.

To capture the displacement and strains suffered by the composite solution during the tensile tests a 2D-DIC approach was used. The acquisition of these images was carried out by means of the DIC prototype developed by García-Martin et al. [36]. This

Table 1
Technical characteristics of fibers CC 200 T-120®.

Mechanical properties	Values
Thickness (mm)	0.32
Density (warp × weft) (end/cm)	1.76
Tex (warp × weft)	500 × 500
Width (cm)	120 ± 1
Weight (g/m^2)	200 ± 5
Weight per roll (kg)	110
Tensile strength (MPa)	3530
Elongation at maximum tensile strength (%)	1.5

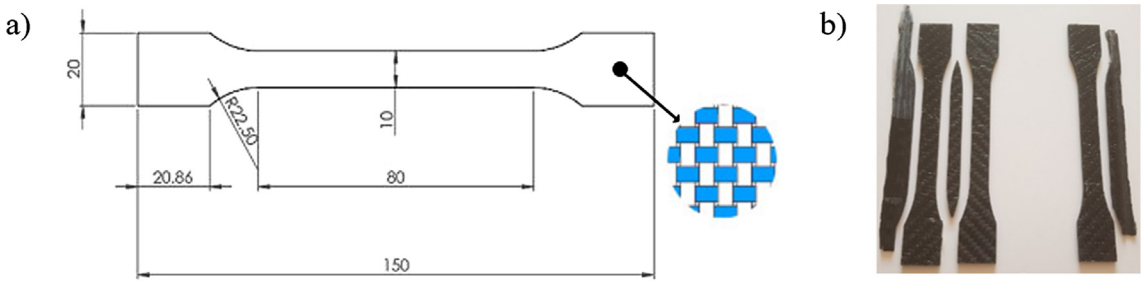

Fig. 1. Manufacturing process: a) dimensions of the tested specimens in mm and; b) image of the specimens.

prototype is composed of a high resolution camera Canon EOS 700D with a 60 mm prime macro-lens and a PLC connected with the load cell.

Once the images were acquired, a standard DIC protocol was applied in order to obtain the full field of displacements and strains. During this stage, the Region Of Interest (ROI) of each image was split into subsets [46] which allow the images to be tracked through the Zero mean Normalized Cross-Correlation (ZNCC) index due to its robustness [47]. During this tracking stage, it was assumed that each subset could suffer a deformation result of the linear combination of six degrees of freedom (translation, elongation and shear deformation in the x and y axis) (Fig. 2) (Eqs. (1) and (2)) for which the basic form of displacement of a subset is $\left(u, v, \frac{\delta u}{\delta x}, \frac{\delta u}{\delta y}, \frac{\delta v}{\delta x}, \frac{\delta v}{\delta y}\right)^T$.

$$x' = u + \frac{\delta u}{\delta x}\Delta x + \frac{\delta u}{\delta y}\Delta y \tag{1}$$

$$y' = v + \frac{\delta v}{\delta x}\Delta x + \frac{\delta v}{\delta y}\Delta y \tag{2}$$

where x' and y' are the final displacements of the subset; u and v are the displacements components of the subset center P; Δx and Δy are the distance between the initial center's subset and the final position and; $\frac{\delta u}{\delta x}$, $\frac{\delta u}{\delta y}$, $\frac{\delta v}{\delta x}$, $\frac{\delta v}{\delta y}$ are the displacement gradients of the subset.

Complementary to the ZNCC index, and with the aim of obtaining sub-pixel accuracy, a refinement stage was carried out by means of the following strategies: i) a bi-quantic b-spline interpolation scheme to pass from the discrete values of the images (0–255) to a continuum space and; ii) the Inverse Composition Gauss-Newton method for the minimization of the cost function that match the reference subset with the deformed one. For more details about the algorithms used the reader is referred to [47].

The procedure previously shown was reproduced in all the image's subsets allowing us to obtain a full-field of displacements. The strains of the specimens were calculated by means of the Green-Lagrangian strain tensor using the gradients obtained during the evaluation of the displacements [36]. In order to obtain the full field strain, this procedure was applied throughout ROI.

The success of the tracking carried out during the DIC approach strongly depends on the random intensity distribution of the ROI, wich must present the following features: distinct, unique, non-periodic and stable grayscale [48]. Due to the absence of a proper gray variation on the specimen's surface, it was necessary to apply an artificial Speckle pattern using the approach defined by Garcia-Martin et al. [36]. This strategy allows us to obtain a suitable Speckle pattern through the perturbation of a regular circular grid, wich was printed and applied with the help of an elastic prime over the specimen surface.

Apart from the considerations previously shown, the images captured by the sensor suffer from lens distortion that could be considered as another source of error [47]. The minimization of this error requires the removal of the these radial and tangential distortions. Therefore, the present case applied the calibration procedure proposed by Vo et al. [49].

In order to guarantee the accuracy and quality of the data obtained with the DIC approach, it is mandatory that all previously determined steps are carried out by skilled technicians. First, the prototype must be properly configured to synchronize all data. A bad Speckle pattern with insufficient contrast could cause the subsets not to be detected correctly and the correlation was not performed. In addition, all parameters have to be defined according to the test configuration for the correlation algorithm runs properly. Finally, the calibration process has to be carefully carried out in order to obtain a high accuracy in the results, since a bad calibration could cause incoherent displacements and strains.

Table 2
Servosis ME-405/50/5 technical specifications.

Maximum Load	500 kN
Load Cell	REP Transducer Type TC4 50 kN
Grip	MTS Model XSA304A

2.3. Numerical strategy for the reliability analysis

As stated in the Introduction, the main goal of the reliability analysis is to find the probability function of a mechanical system under the influence of different uncertainties. These uncertainties could be considered at material (random variables and random field) or ply level (layer-wise random variable). For the present study, we considered the mechanical uncertainties of the composite solution at ply level. These uncertainties were extracted by means of the DIC approach previously described. The evaluation of the probability function was carried out through the Monte Carlo (MC) approach following the next formulation (Eq. (3)). The input data required for the MC simulation was obtained combining a finite element modelling simulation with a surrogate metamodeling strategy, allowing reduction of computational costs as well as the estimation of the Sobol' indices for the sensitivity analysis of the mechanical solution. The proposed workflow was carried out with different number of plies until the probability of failure of the model was less than the minimum threshold of probability of failure (optimal solution) (Fig. 3). This failure threshold corresponds to the reliability target (β) which guarantees the safety of the model.

$$P_f = Prob[G(Y) \leqslant 0] = \int_{G(Y)\leqslant 0} p_y(Y)dY \tag{3}$$

where P_f is the probability of failure; G is the performance function; Y is the variable's vector and p_y is the joint probability density function.

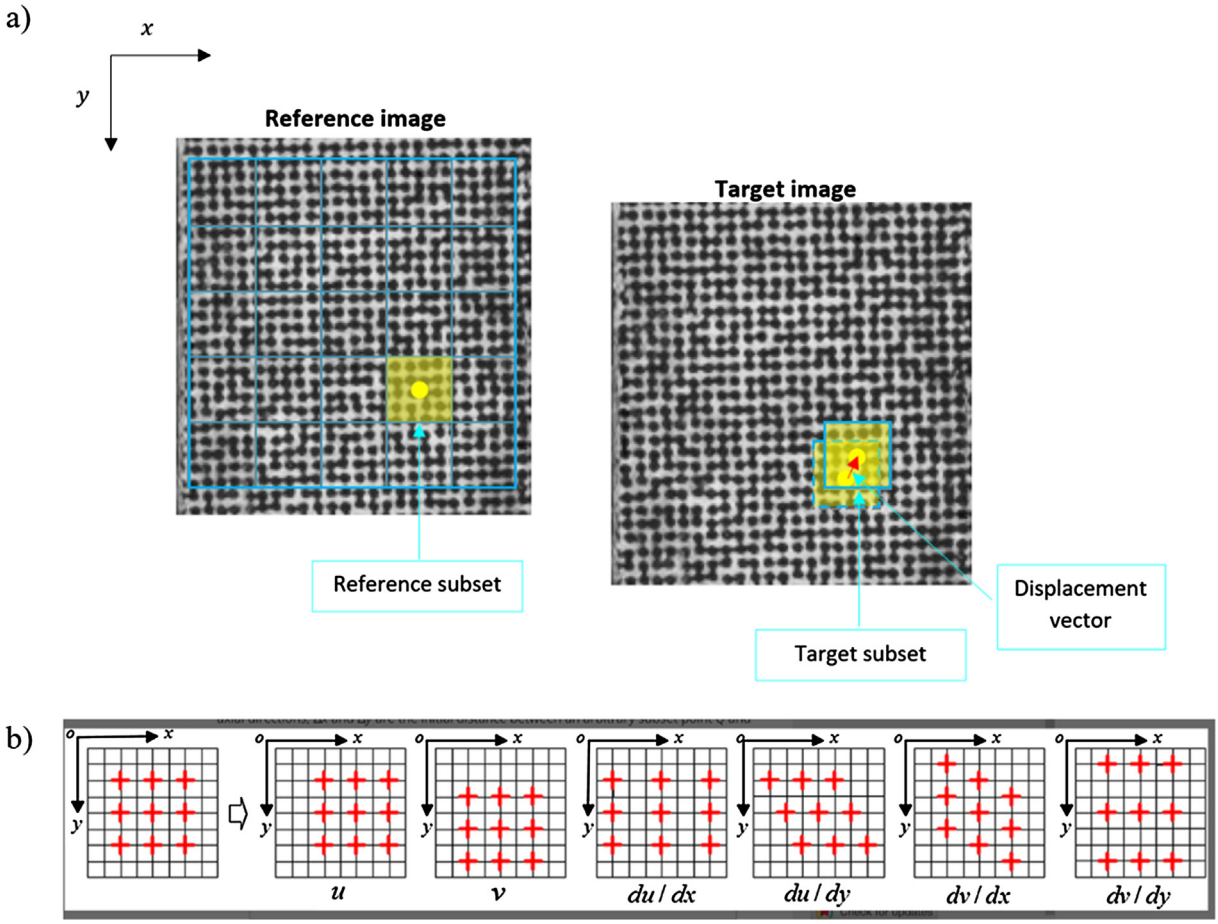

Fig. 2. Graphical representation of the DIC approach: (a) evaluation of the displacement suffered by a subset and (b) degrees of freedom considered during the displacement analysis.

2.3.1. Definition of the performance function for the reliability analysis: the Tsai-Wu failure criterion

Among the different methods able to simulate the failure of composite solutions, the Tsai-Wu failure criterion is one of the most used in the literature [7,12,14,50]. This criterion assumes that the failure of a composite solution takes places when the Failure Index (FI) (Eq. (4)) is higher than 1 [51].

$$FI = F_1\sigma_1 + F_2\sigma_2 + F_3\sigma_3 + F_{11}\sigma_1^2 + F_{22}\sigma_2^2 + F_{33}\sigma_3^2 + 2F_{12}\sigma_1\sigma_2 + 2F_{23}\sigma_2\sigma_3 + +2F_{31}\sigma_3\sigma_1 + F_{44}\sigma_4^2 + F_{55}\sigma_5^2 + F_{66}\sigma_6^2 \leq 1 \quad (4)$$

where:

$F_1 = \frac{1}{X_T - \frac{1}{X_C}}$	$F_2 = \frac{1}{Y_T - \frac{1}{Y_C}}$	$F_3 = \frac{1}{Z_T - \frac{1}{Z_C}}$
$F_{11} = \frac{1}{X_T X_C}$	$F_{22} = \frac{1}{Y_T Y_C}$	$F_{33} = \frac{1}{Z_T Z_C}$
$F_{44} = \frac{1}{S_{yz}^2}$	$F_{55} = \frac{1}{S_{zx}^2}$	$F_{66} = \frac{1}{S_{xy}^2}$
$F_{12} = \left(-\frac{1}{2}\right)\sqrt{F_{11}F_{22}}$	$F_{23} = \left(-\frac{1}{2}\right)\sqrt{F_{22}F_{33}}$	$F_{31} = \left(-\frac{1}{2}\right)\sqrt{F_{33}F_{11}}$

$X_T \equiv$ Tensile strength
$X_C \equiv$ Compressive strength
$Y_T \equiv$ Tensile strength in the transversal isotropic surface
$Z_T \equiv$ Tensile strength in the transversal isotropic surface
$Y_C \equiv$ Compressive strength in the transversal isotropic surface
$Z_C \equiv$ Compressive strength in the transversal isotropic surface
S_{xy}; S_{yz}; $S_{zx} \equiv$ Shear strength in the transversal isotropic surface

According to the formulation previously exposed, the performance function of a composite solution in terms of Tsai-Wu failure criterion could be expressed as (Eq. (5)). Taking this into consideration, the composite solution is operating in the safety range if $G > 0$ and in the failure state if $G < 0$, and the surface $G = 0$ is the limit state of the solution.

$$G = 1 - FI \quad (5)$$

where G is the performance function and FI is the failure index obtained from the Tsai-Wu criterion.

2.3.2. Metamodeling strategy

The proposed methodology considers the use of the MC sampling method for solving the probability of failure of the system (Eq. (3)). To achieve reliable results, thousands of simulations are required for solving the problem. The computational cost of this task is unacceptable most of the times, so it is necessary to establish an alternative that offers reliable results with a lower computational cost. In this context, the so-called surrogate models or metamodels allow the Input-Output response of a complex system to be approximated with a low number of inputs thanks to its compactness and analytical scalability. Within this context, one of the most robust and used metamodeling strategies is the Polynomial Chaos Expansion (PCE) [52], especially in the propagation of uncertainties in engineering applications [53].

Initially developed by Wiener [54], the PCE is a stochastic metamodeling strategy that approximates the behaviour of a system by means of a spectral representation of random variables in terms of a set of multivariate polynomials. This method assumes that the physical model, in this case the numerical simulation, can be represented as a finite variance model, f(X), whose input x is a random

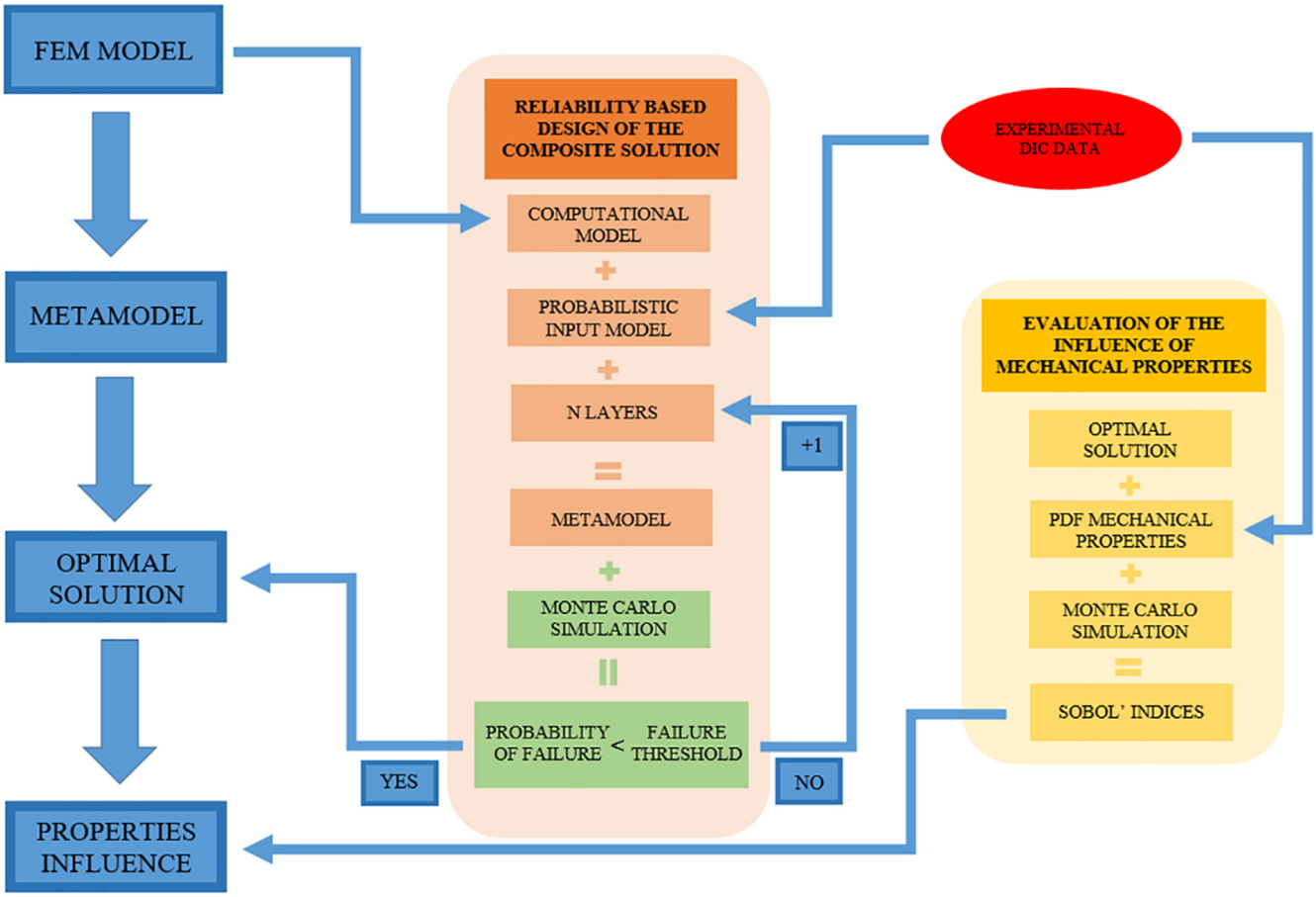

Fig. 3. Workflow adopted for the reliability analysis.

vector of independent and constrained variables $X \epsilon R^M$. The independence of the input parameters allows us to build these polynomials as a tensorization of univariate polynomials with respect to the marginal PDF's and where the mathematical equation can be summarized as follows (Eq. (6)).

$$Y \approx f(X) = \sum_{\alpha \in A} \gamma_a \varphi_a(X) \tag{6}$$

where $\alpha = \{\alpha_1 \cdots \alpha_M\}$ is the multi-index, $A \subset N^M$ is a set of indices for the multivariate orthonormal polynomials, γ_a are deterministic coefficients to be computed and $\varphi_a(X)$ are multivariate orthonormal polynomials.

The estimation of the coefficients exposed in (Eq. (6)) was carried out by means of a least square minimization problem between the vector of random inputs (X) and the model responses (Y) as follows (Eq. (7)):

$$\varphi_\alpha = argmin \frac{1}{N} \sum_{i=1}^{N} \left[\gamma^{(i)} - \sum_{\alpha \in A} \gamma_\alpha \varphi_a \left(x^{(i)} \right) \right]^2 \tag{7}$$

In order to overcome a possible over-fitting situation in the presence of high-dimensional inputs, the proposed methodology uses the adaptive sparse PCE based on the least angle regression proposed by Blatman and Sudret [55]. This method applies the

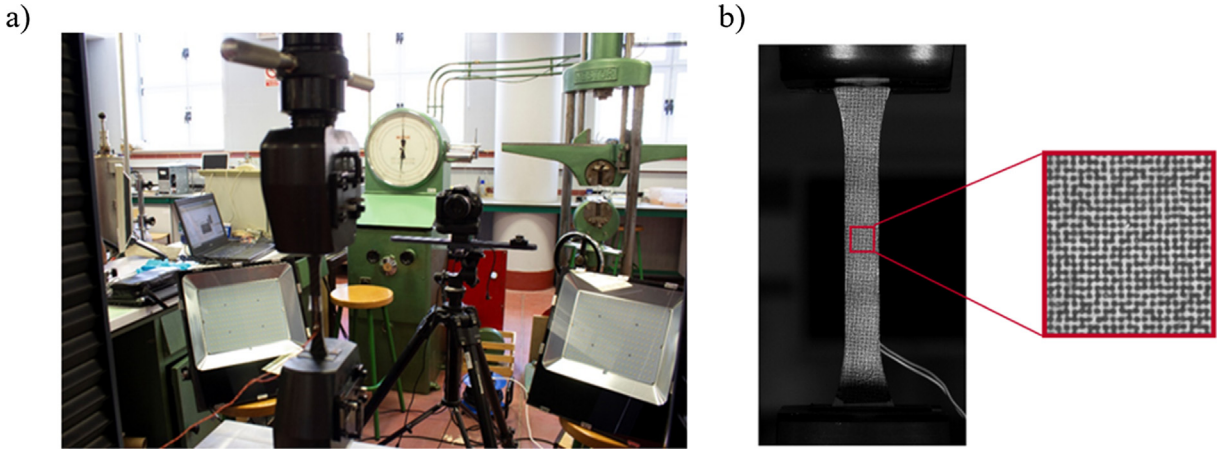

Fig. 4. Digital Image Correlation campaign: a) set-up used and; b) detail of the Speckle pattern applied.

Table 3
Internal parameters obtained during the calibration of the camera. Unit*: pixel.

Parameter		Initial	Refined
Focal length*	f_u	1.36286×10^4	1.5206×10^4
	f_v	1.36286×10^4	1.5208×10^4
Principal point*	u	7.2084×10^2	2.5118×10^3
	v	1.3378×10^3	2.0986×10^3
Radial distortion coefficients	a_0	0	-8.5316×10^{-2}
	a_1	0	3.3055×10^{-1}
	a_2	0	1.0130×10^{1}
Tangential distortion coefficients	p_0	0	-3.0724×10^{-3}
	p_1	0	1.5447×10^{-2}

least angle regression algorithm [56], based on a regularized version of the Eq. (7), to obtain a sparse PCE metamodel. This strategy proves to be very effective in engineering problems with high dimensions [55].

It is worth mentioning that all the metamodels are built from a limited number of inputs coming from the Design of Experiments (DoE). Thus, it is essential to assess the quality of the computed surrogate model. To this end, we propose to be use the modified version of the Leave-one-out error [57] (Eqs. (8) and (9)). This metric of error offers a good compromise between fair error estimation and affordable computational cost.

$$LOO\ error = \frac{1}{N}\sum_{i=1}^{N}\left(\frac{Y\left(X^{(i)} - f^{\,PCE}\left(X^{i}\right)\right)}{1-h_i}\right)^2 \tag{8}$$

$$LOO\ error^{*} = LOO\ error * \left(1-\frac{cardA}{N}\right)^{-1}\left(1+tr\left(\varphi^T\varphi\right)^{-1}\right) \tag{9}$$

where $Y\left(X^{(i)}\right)$ is the computational model; $f^{\,PCE}\left(X^{(i)}\right)$ is the surrogate model obtained from a specific DoE with N samples; h_i is the i-th diagonal term of matrix $A\left(A^TA\right)^{-1}A^T$; A the experimental matrix; *card A* is the number of terms in the truncate series and; $\varphi = \left\{\varphi_{ij} = \varphi_j(x^{(i)}),\quad i = 1,\cdots,N;\quad j = 1,\cdots,cardA\right\}$.

The reduced computational cost of the surrogate metamodeling strategy allows the application of the MCS for different purposes. According to this, it is possible to calculate the influence of each

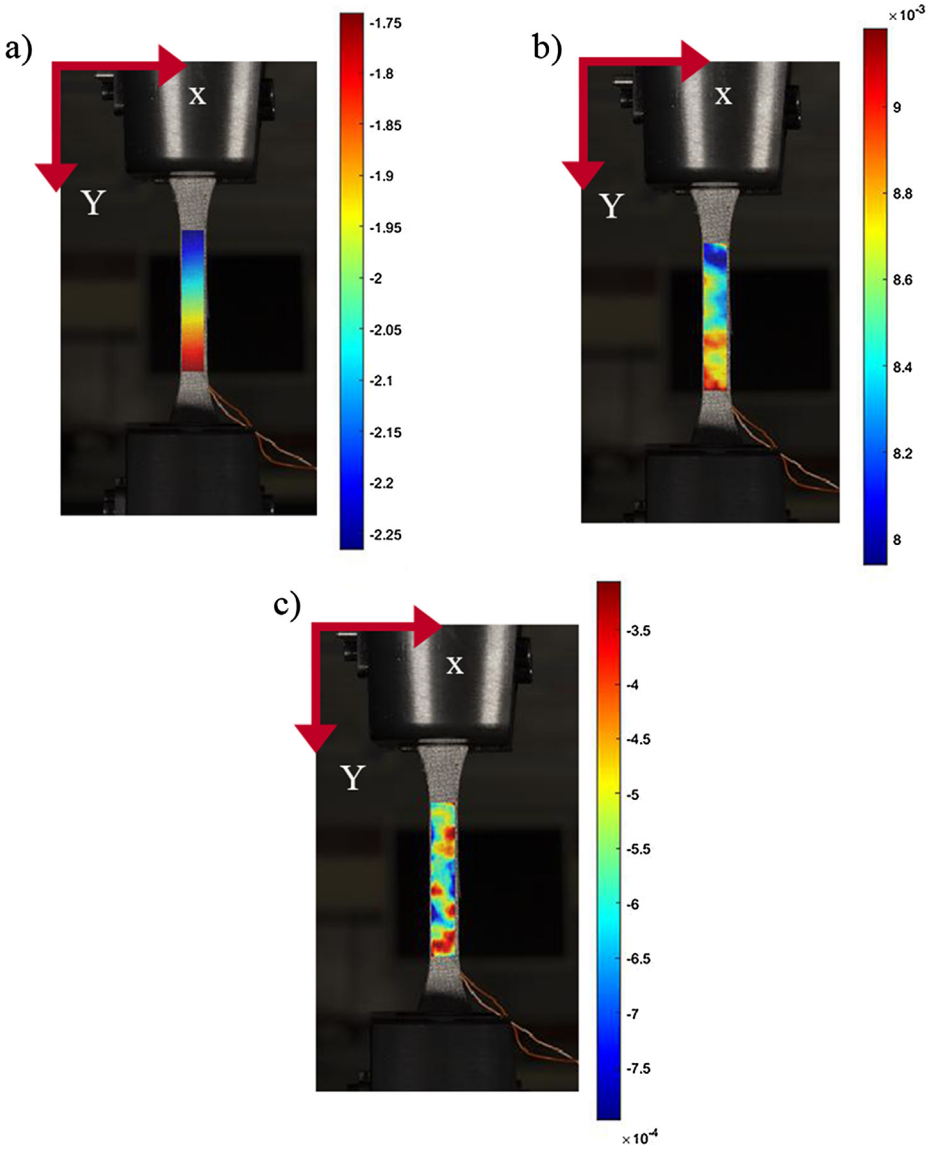

Fig. 5. Displacements and strains obtained by the 2D-DIC approach: a) displacements (Y) in mm; b) strains (Y) in mm/mm and c) strains (X) in mm/mm.

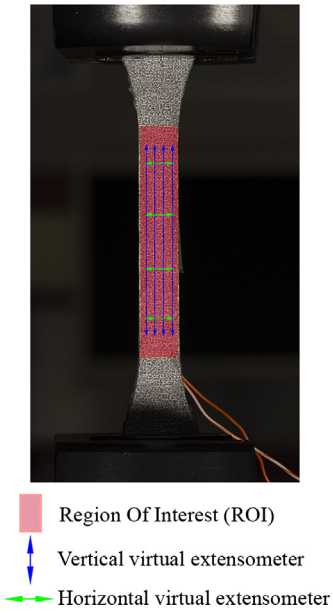

Fig. 6. Extraction of the mechanical parameters: evaluation of the Young's modulus and Poisson's ratio by means of virtual extensometer.

input in the final result of the model. Within this context one of the most used strategies is the estimation of the Sobol' indices. These indices assume that the variance of the model (output) can be described as a sum of the variances of the inputs (Eq. (10)). The normalized version of each variance with respect to the total one allows us to obtain de Sobol' indices with different orders (from 1 to 2^{n-1}) (Eq. (11)). The sum of these indices is the total Sobol' index whose value is equal to 1.

$$V(Y) = \sum_i V_i + \sum_i \sum_{j>i} V_{ij} + \sum_i \sum_{j>i} \sum_{k>j} V_{ijk} + \cdots V_{123..N} \tag{10}$$

where $V(Y)$ is the variance of the model; $V_i = V(E(Y|X_i))$ is the first order partial variance; $V_{ij} = V(E(Y|X_i,X_j))$ is the second order partial variance, etc.

$$S_i = \frac{V_i}{V(Y)}, \quad S_{ij} = \frac{V_{ij}}{V(Y)}, \text{ etc} \tag{11}$$

where S_i is the first order Sobol' index and S_{ij} is the second-order Sobol' indices.

3. Experimental results

3.1. Analysis of the roll wrapping solution by means of 2D-DIC

3.1.1. Test setup

A total of fifty-one tensile tests were carried out following the BS EN ISO 527-5:2009 guidelines [45]. The images for the DIC analysis were acquired each 400 N of traction force increment, taking the first image without load in order to obtain the reference image. Previously to the tests, a preparation stage was carried out with the aim of optimizing the results obtained during the tensile tests. This stage comprised the following steps: i) definition of the ground sample distance (GSD) as well as the aperture of the lens; ii) application of the Speckle pattern and; iii) the geometrical calibration of the camera.

The images were acquired with the same camera configuration used by García-Martin et al. [36]. Taking these values into account, a Speckle pattern was designed using the methodology proposed in Section 2.2, using a diameter of 0.324 mm and a step of 0.432 mm and obtaining a covering factor of 44% [58]. Finally, this pattern was printed and applied on the specimen surfaces by means of an elastic prime (Fig. 4). The quality of the pattern was evaluated through the Mean Intensity Gradient (MIG) value [59], obtaining an average value of 50. This value was considered acceptable taking into account the method used [59].

For the camera calibration we used the calibration approach defined in Section 2.2, acquiring a total of 22 images. The following inner parameters were obtained (Table 3).

3.1.2. Displacement and strain results

In order to obtain the displacamet and strain on each test specimen, DIC approach defined in Section 2.2 was carried out with the open-source software Ncorr [60]. A subset size of 20 × 20 pixels and a 35% overlap (step of 7 pixels) were considered to ensure a proper DIC configuration [46], obtaining a full fiel displacement and strains in all the ROI (Fig. 5).

Taking into consideration the test set-up, the state of stresses along the central area (ROI area) could be considered to be constant. Therefore, if the material is homogeneous, the expected maximum principal strains will be reached at the same time in all the ROI. However, the results of the DIC tests revealed a heterogeneous distribution of the strains in the longitudinal and transverse directions and thus the presence of different mechanical properties along the composite structure. These heterogeneities could be attributed to local variations during the manufacturing process [36].

3.1.3. Extraction of the PDF functions

As stated in Section 2.3, the reliability analysis requires prior knowledge of the probability density functions of the material's variables. The population of each variable evaluated by means of the DIC approach was extracted during the next strategy (Fig. 6) (Table 4): i) creation of several virtual extensometers to evaluate the Young's Modulus and Poisson's ratio and; ii) extraction of maximum principal strain for the evaluation of the ultimate capacity of the material.

With the aim of obtaining a wide population, eight virtual extensometers were placed in each specimen. Four of them were placed vertically (y axis) and other four were placed horizontally (x axis) (Fig. 6). In this way, a total of 204 values were obtained for the Young's Modulus and Poisson's ratio.

This wide population allowed to calculate a significant average value and covariance associated with each of the parameters. In

Table 4
Results obtained from the mechanical characterization of the specimens using DIC approach.

Composite solution evaluated					
Parameter	Number of data	Mean	Covariance (%)	Lower bound	Upper bound
E-Young's modulus (GPa)	204	50.7088	4.07	45.0583	57.0596
v-Poisson's ratio (–)	204	0.0574	41.95	0.0138	0.1462
T-Maximum principal tensile (MPa)	51	402.5128	8.33	309.5652	461.5762

Table 5
Goodness of fit (GOF) probability; N-Normal, LN-Lognormal, W-Weibull, G-Gamma; 0-Accept and 1-Reject. Chi-Square (Chi), Kolmogorov-Smirnov (KS) and Anderson-Darling (AD) tests of the Young's Modulus (E), Poisson's ratio (ν) and Maximum principal tensile (T).

PDF	N			LN			W			G		
GOF	Chi	KS	AD	Chi	KS	AD	Chi	KS	AD	Chi	KS	AD
E	1	0	0	0	0	0	1	1	1	0	0	0
ν	1	0	1	0	0	0	1	0	0	0	0	0
T	0	0	0	0	0	0	0	0	0	0	0	0

Table 6
Probabilistic distribution functions of the Young's Modulus (E), Poisson's ratio (ν) and Maximum principal tensile (T) of the specimens.

Parameter	Distribution	μ (Log-Normal)/A (Weibull)	σ (Log-Normal)/B (Weibull)
E	Log-Normal	3.9253	0.0405
ν	Log-Normal	−2.9422	0.4176
T	Weibull	417.0948	14.8402

this sense, it is worth mentioning the high value of the covariance associated with the Poisson's ratio. Generally high covariance values of the Poisson's Ratio are obtained in comparison with those of other parameters [61,36]. These high values are mainly due to the importance of fiber alignment in the manufacturing process as well as the low average value of the Poisson's ratio of the CRFP.

The reliability analysis approach proposed in Section 2.3 allow quantifying the uncertainty of the mechanical properties previously obtained. In order to introduce this uncertainty, it was necessary to adjust these data to a probabilistic distribution.

Along with this test, the goodness-of-fit tests of Chi-Square, Kolmogorov–Smirnov and Anderson-Darling were performed. These techniques allow us to accept or reject the hypothesis that mechanical properties are drawn from populations with a specified distribution [62]. Finally, a curve fit method was performed with the aim of obtaining the PDFs.

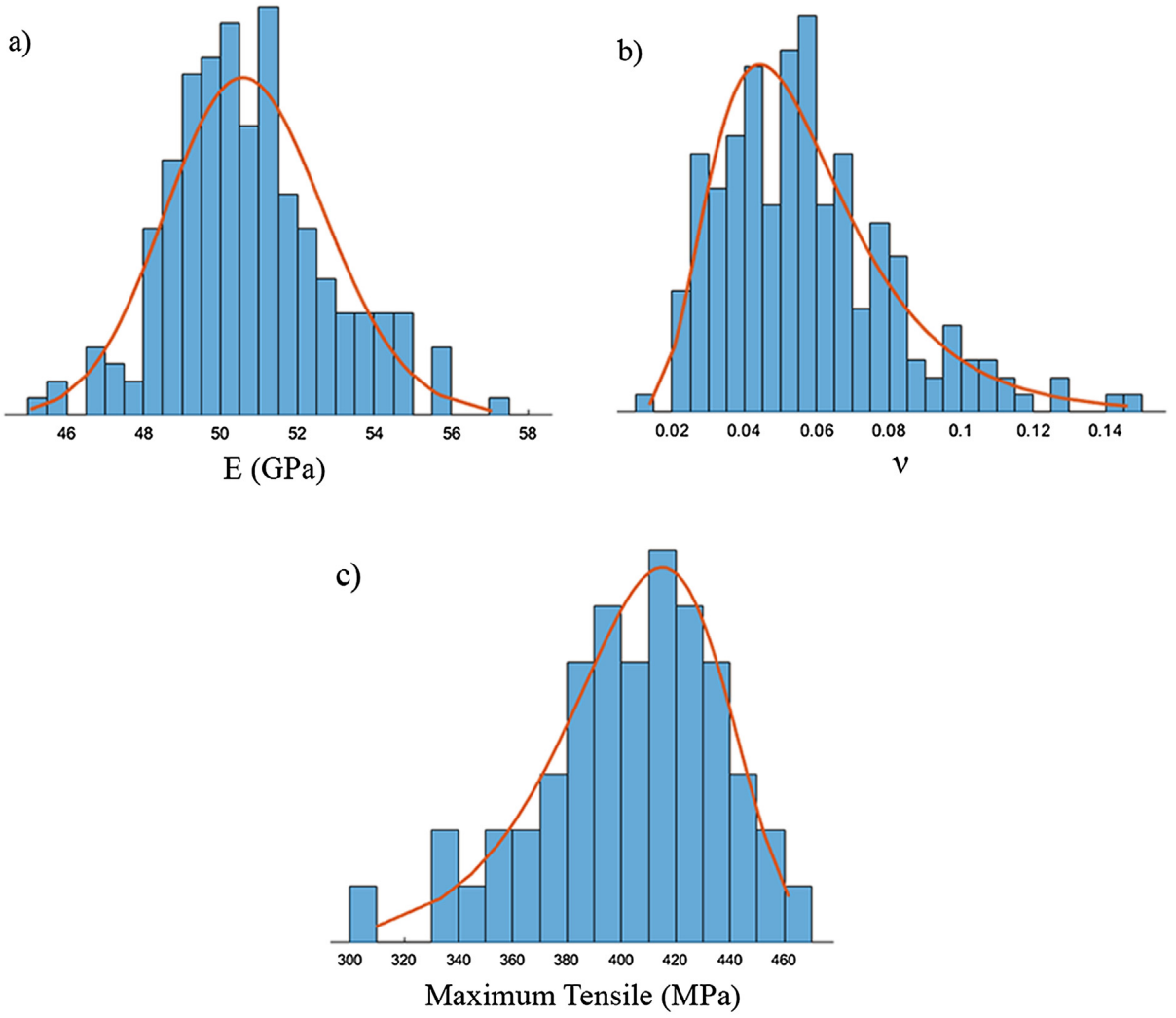

Fig. 7. Graphical representation of the PDFs of each parameter: (a) Log-Normal distribution of the Young's modulus *(E)*; (b) Log-Normal distribution of the Poisson's ratio *(ν)* and (c) Weibull distribution of the maximum principal tensile *(T)*.

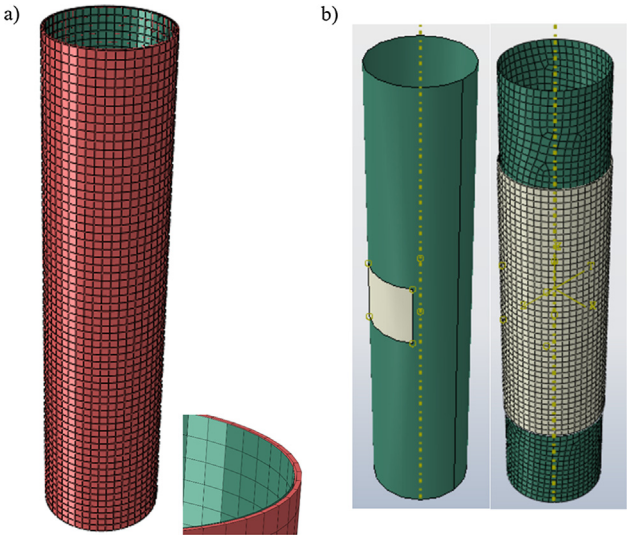

Fig. 8. Numerical meshes used: a) new composite steel pipe and; b) retrofitting of a corroded steel pipe.

Table 7
Results of probability of failure (P_f) and reliability index (β) obtained during the reliability analysis of the composite pipe with 10, 11, 12, 13, 14 and 15 layers.

Number of layers	P_f	β
10	0.5061	0.0154
11	0.1661	0.9696
12	0.0480	1.6645
13	0.0132	2.2200
14	0.00356	2.6912
15	0.00108	3.0645

The candidate PDFs considered were Normal, Log-Normal, Weibull, and Gamma. The acceptance/rejection of distribution is provided in Table 5 where zero indicates acceptance of assumed distribution parameters, and unity indicates rejection. As shown in Table 5, for some parameters there are several candidate PDFs which pass all tests.

Along with these statistical tools, the physical considerations of the parameters were taken into account, obtaining a Log-Normal distribution for the Young's Modulus and Poisson's Ratio and a Weibull distribution for the maximum principal tensile stress (Table 6 and Fig. 7). These curves are consistent with those obtained in similar experiments [61].

3.2. Definition of the numerical models

Taking into account the main applications of the roll-wrapping technique, two numerical models were considered for the reliability analysis: i) the design of a new composite pipe and; ii) the repair of a corroded steel pipe (Fig. 8). Both numerical simulations were carried out in the FEM software ABAQUS 2019®.

On the one hand, the composite pipe was modelled considering the following parts: i) a non-structural polymer liner with 2 mm of thickness; ii) a composite wrap made up of several composite layers with 0.32 mm of thickness. The wrap part was meshed as a continuum shell with reduced integration and eight nodes SC8R elements, while the liner was meshed with in-plane general purpose shell elements with four nodes, S4R. Convergence analyses were done in both models in order to obtain a mesh size which could give good precision results without penalizing enormously the time needed to run the models. This is a paramount aspect to consider because the models had to be repeated 200 times in order to obtain the surrogate models, as it was explained in Section 2.3.2. So, convergence studies were performed using elements between 20 and 1 mm size. It was observed that using elements smaller than 10 mm the results did not improved significantly, but the sizes of the whole models and the time to run them grew exponentially. Finally, a 10 mm size element was considered enough precise for both models. For the loading and boundary conditions, we used an internal pressure on the inside wall of the pipe of 11.2 MPa and plane strain boundary constraints. Under these conditions the principal stresses which works in the pipe were the hoop tensile stresses [63].

On the other hand, we also considered a corroded steel pipe retrofitted with the composite solution exposed in Section 2.1 and by means of roll-wrapping technology. In this sense, the numerical model was made up of the following parts: i) a steel pipe with 4 mm of thickness; ii) a corroded area on which the effective thickness is 2 mm (half of the initial one); iii) a non-structural putty layer and; iv) a roll-wrapping solution made up of different composite layers of 0.32 mm thickness each. It is worth mentioning that the loads and boundary conditions were the same as those previously exposed.

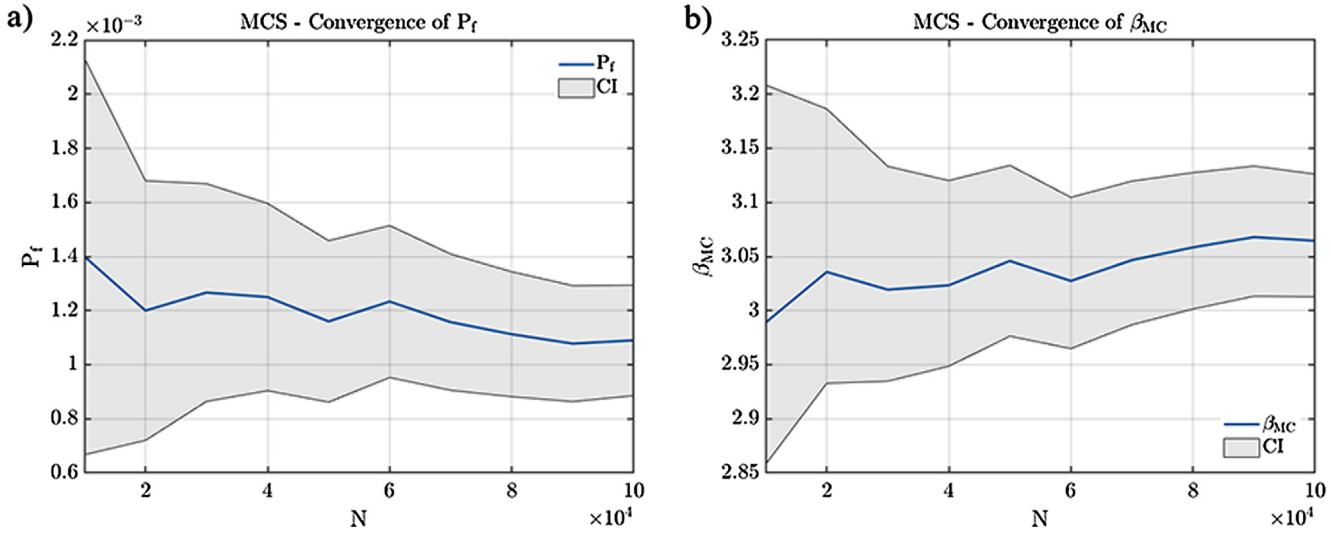

Fig. 9. Convergence of the P_f and β during the Monte Carlo Simulation.

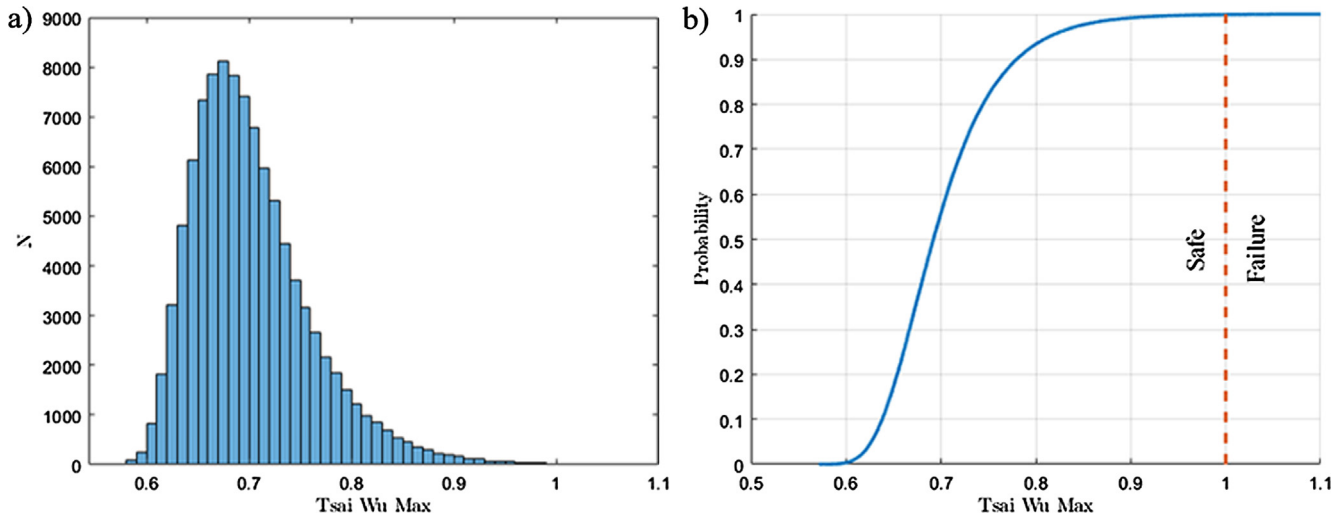

Fig. 10. Reliability analysis of the 15 layer's model: a) PDF function and; b) CFD function.

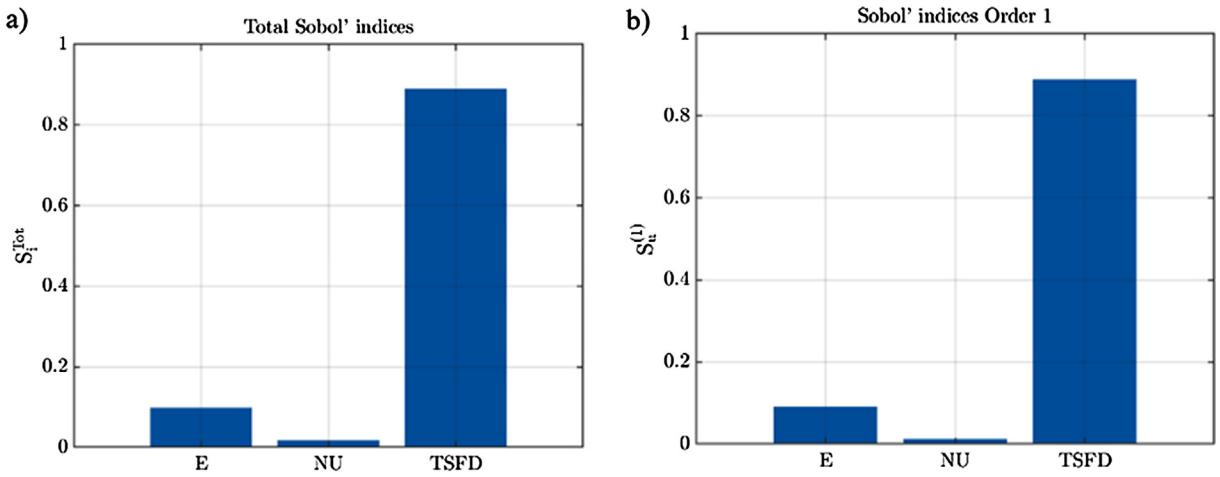

Fig. 11. Results obtained during the sensitivity analysis: a) Total Sobol' indices and; b) First-order Sobol' indices.

The number of layers in each numerical simulation were determined during the reliability analysis. To this end, the iterative approach defined in Section 2.3 was applied, defining a maximum probability of failure of 0.00135 (reliability index of 3.0). This strategy was carried out in the mathematical software MATLAB with the assistance of the open-source library UQLab [64].

3.3. Results obtained during the design of the new composite pipe

With the aim of obtaining the optimal number of layers for the composite pipe previously shown, an iterative reliability analysis proposed in Section 2.3 was carried out. During each iteration a PCE of the model response was built considering as random inputs the mechanical variables of each layer namely: i) Young's Modulus; ii) Poisson's ratio and; iii) tensile strength. The PDFs of these variables were those obtained in the DIC evaluation (Fig. 7). Throughout this process we used the Latin Hypercube Sampling method to create the DoE [65]. This technique is a popular method that allows us to obtain a random DoE ensuring the uniformity of each sample in the domains of the inputs. From the present study case several sizes of the DoE were used to build the metamodel. The accuracy of the metamodel was evaluated by means of the LOO error exposed in (Eqs. (8) and (9)). The metric of this error was complemented by a cross correlation on which we used a different DoE with the same size. The sparsity of the metamodel was carried out by varying the maximum degree of the polynomials from 1 to 20, where the optimal degree was selected according to the smallest LOO error.

After a total of 15 iterations the reliability analysis found a solution which satisfied the failure criteria. In this situation the degree of the polynomials was 5 with an associated LOO error of 0.0047 and a cross-validation error of 0.005.

According to the numerical results obtained, it was necessary to use a total of 15 CFPR layers to satisfy the failure criteria previously defined ($P_f < 0.00135$, $\beta > 3$) (Table 7 and Fig. 9). In this situation, the solution has a probability of failure of 0.00108 and a reliability index of 3.0645 (Fig. 10).

In order to understand which mechanical variables are the most relevant in the safe design of the composite pipe, a Sobol sensitivity analysis was carried out. To this end a new MCS was performed, using in this context a total of 500,000 simulations. During this process it was assumed that all the layers have the same mechanical properties according to the PDF obtained during the DIC analysis (Fig. 7). The figure indicates that the tensile strength of the material is the most relevant mechanical parameter in the safety of the solution followed by the Young's Modulus. This mechanical

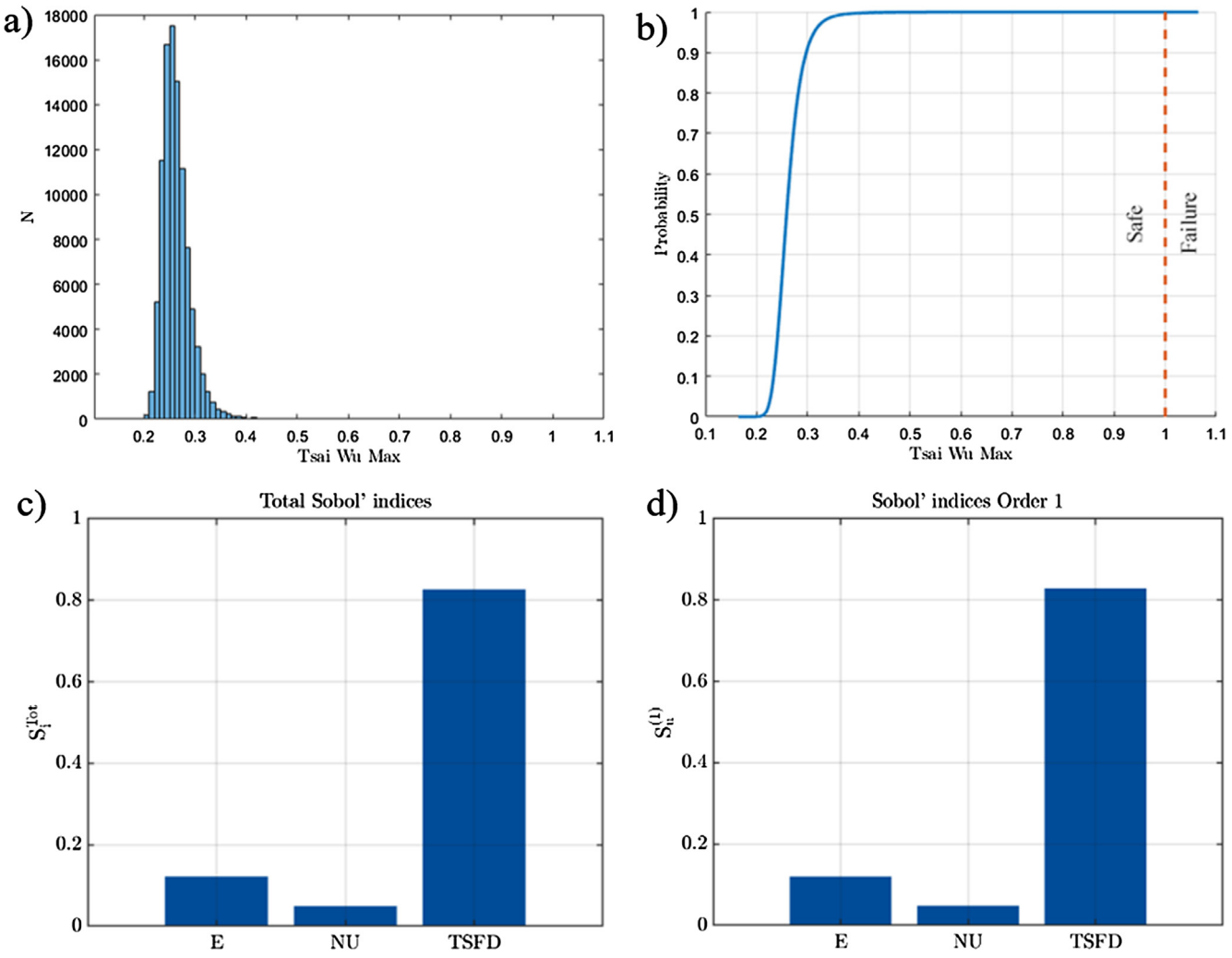

Fig. 12. Results obtained during the reliability analysis of the corroded pipe retrofitted with 4 layers of CFPR: a), b) PDF and CFD functions and; c), d) Sobol' indices.

property explains 89.00% of the total variance (Fig. 11). The great similarity between the first and the total Sobol-indices highlights the absence of a second-order effect.

3.4. Reliability evaluation of a corroded steel pipe retrofitted with CFPR

Apart from the design of new composite pipes, another relevant application of the method could involve the retrofitting of existing steel pipes. Within this context the most common damage is the corrosion of the pipe which reduces the resistance section of it. According to this, and considering the numerical model of the corroded steel pipe defined in Section 3.2, the proposed iterative reliability analysis was performed. During this analysis we used as inputs the mechanical variables obtained by DIC (Fig. 7) as well as the thickness of the corroded area. The PDF of this input was assumed uniform, varying from 0% (totally corroded) to 100% (no corrosion).

The results of the iterative reliability analysis showed that the minimum number of layers required to fulfil the safety requirements (P_f < 0.00135, β > 3) are 4. With this set-up the probability of failure is $1x10^{-5}$ and the reliability index is 4.26, using MCS with 10^5 simulation (Fig. 12). These simulations were obtained by means of a PCE metamodel with maximum polynomial degree of 7, a DoE made up by 200 samples and a LOO error of 0.005. This error is similar to the error resulting from the cross-validation estimated in 0.003.

It is worth highlighting that the thickness of the corroded part is a critical parameter in this type of reliability analysis, determining the number of layers required to retrofit the steel pipe. Hence, it is neccessary to know the minimum thickness of steel for which the 4 CFPR layers fulfil the safety requirements. To this end, a constrained optimization procedure was carried out using as cost function the thickness of the corroded part and a probability of failure of 0.00135, corresponding to a reliability index of 3. In order to achieve this result, the proposed methodology uses the genetic algorithm described by Goldberg [66]. In this procedure the process starts with an initial population which is repeatedly modified by randomly selecting individuals from the current population and using them as parents to produce the offspring of the next generation. During this process a crossover method creates new individuals on which a mutation strategy ensure that a few genes are modified, exploring a new search space. After several successive generations, the population "evolves" towards an optimal solution [67]. For the present study case the genetic algorithm was based on a population size of 25 individuals with a maximum number of generations equal to 75. For the sequence of creating new populations one individual was chosen to automatically pass to the next generation. The fraction of offspring was established in 75%. In order to obtain the global minimum of the problem, a total of 3 runs were carried out, selecting the run with the best fitness value (Fig. 13). The results of this optimization show that the critical effective thickness is 0.61 mm (15% of the initial section). In this

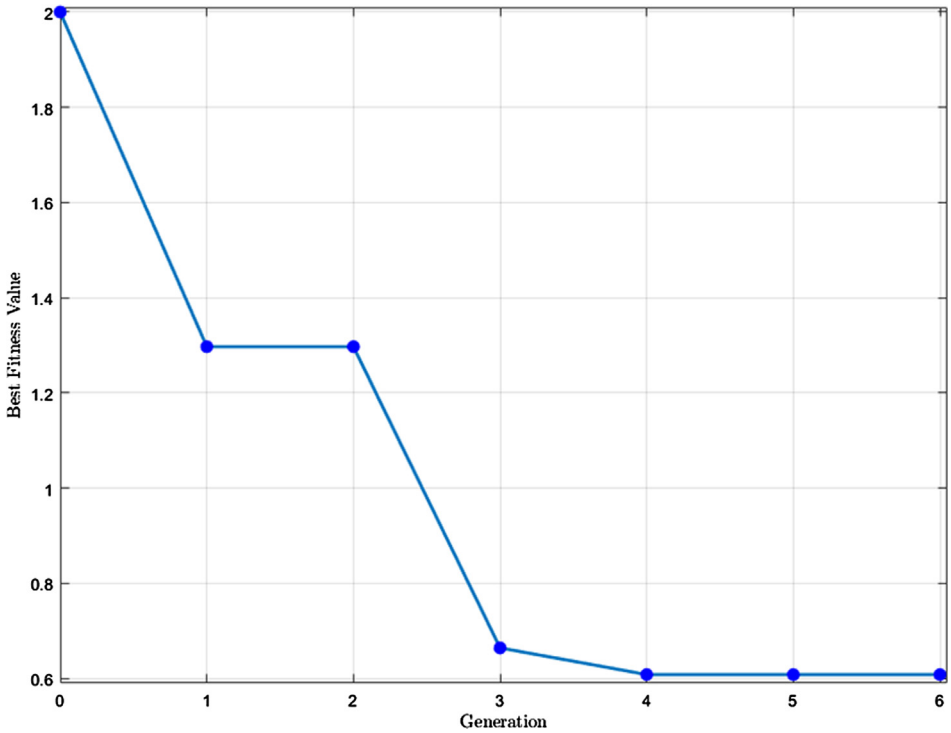

Fig. 13. Convergence plot obtained during the minimization stage.

situation the 4-layer CFPR solution has a reliability index of 3.01 (Figs. 14 and 15).

4. Conclusions

In this paper a new methodology for the reliability analysis of pressurized composite pipes was presented. To this end the method uses the data provided by the digital image correlation approach for the generation of probabilistic distribution function of the different mechanical properties of the composite solution. We subsequently use this data to build a surrogate model of numerical simulation, taking into account the stochastic nature of this type of solution. Therefore, an Adaptive Sparse Polynomial Chaos Expansion was used where the accuracy is evaluated by means of the Leave one Out error. On the one hand, the Digital Image Correlation approach offers a robust and low-cost alternative to traditional contact measurement techniques such as linear variable differential transformers or electrical resistance strain gauges. This alternative is especially attractive in probabilistic approaches for which a large number of inputs are required. In this situation it is possible to exploit the full-field nature of the data by means of virtual extensometers that allows us to extract the mechanical properties of a sample from different locations. On the other hand, the use of an Adaptive Sparse Polynomial Chaos Expansion allows us to mimic the response of a numerical model with great efficiency, requiring a relative low number of inputs to obtain a good Leave one Out error. For example, the two numerical models considered during the present study requires only 200 samples to build an accurate metamodel with an average Leave

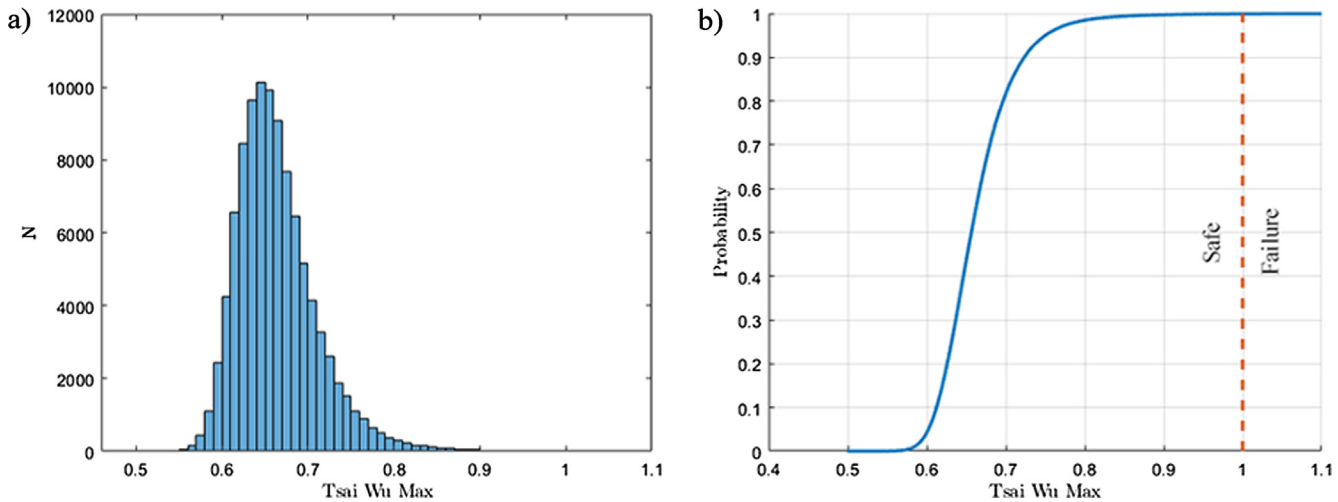

Fig. 14. Results obtained during the reliability analysis of a corroded pipe (15% of the initial section) retrofitted with 4 layers of CFPR: a) PDF and; b) CFD functions.

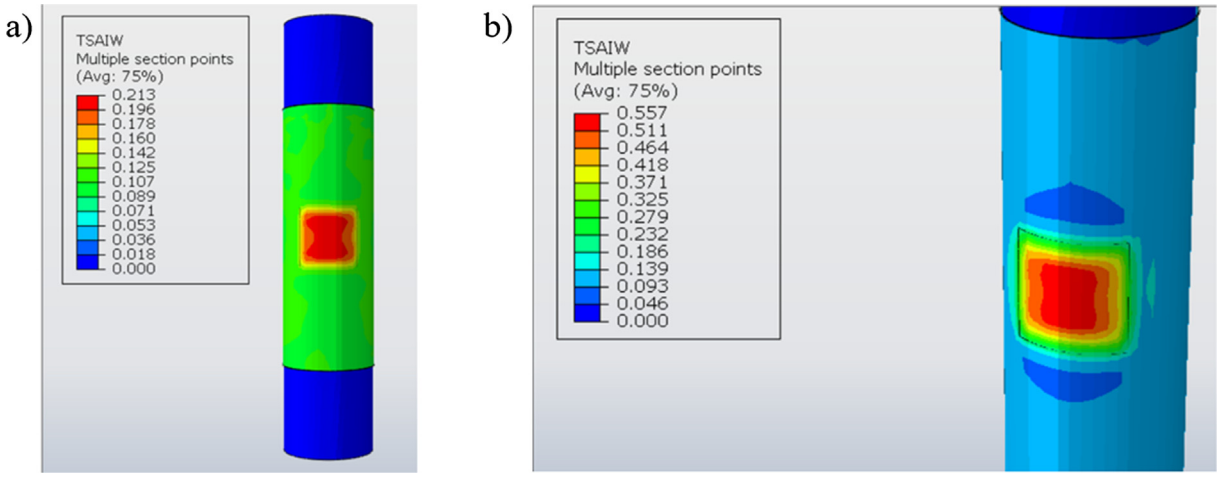

Fig. 15. Distribution of the Tsai-Wu values along the composite solution: a) in a steel pipe with 50% of corrosion and; b) in a steel pipe with 85% of corrosion (maximum value for which the 4-layer CFPR solution is reliable).

one Out Error of 0.005. This metric of error, which is compared with a standard cross validation, is especially efficient since it does not require extra samples to be obtained for the validation. Once the metamodel is obtained, the cost of each evaluation is extremely low, allowing us to carry out a reliability analysis, or even a sensitivity evaluation, by means of the Monte Carlo method. In the context of this study, one numerical evaluation by means of the FEM method requires 25 secs and assumes the investment of 29 days to carry out one Monte Carlo simulation. In contrast, the use of PCE metamodeling requires only 2 h to carry out this simulation (0.3% of the time required to perform this evaluation with FEM simulations alone). Additionally, this surrogate model can be used for optimization purposes (e.g. evaluation of the minimum effective thickness that is able to support a specific composite solution). In this situation the efficient computation cost of the surrogate model allow us to use evolutionary optimization strategies able to find the global optimal of the solution as well as the use of inequalities that introduces uncertainty in the safety evaluation. Within this context the system was able to save 99.7% of the total time required to obtain the optimal solution by means of FEM simulations. All these simulations were carried out in a Intel® XEON E3-1240 v3 processor running at 3.4 GHz with 8 GB RAM DDRII.

Future works will be focused on the use of full-field data provided by the DIC approach to evaluate the uncertainties of the composite solution from a material level by means of Random Field theory. Additionally, the proposed methodology will be used within the context of reliability-based design optimization, integrating minimization algorithms that allow us to estimate the optimal disposition of the composite solution. Also, the proposed method will be applied to other fabrics (plain/satin weave) and materials, where different reinforcements (GDPR) and matrix (especially thermoplastic ones) will be tested.

CRediT authorship contribution statement

Roberto García-Martin: Writing - original draft, Investigation, Funding acquisition. **Jorge López-Rebollo:** Formal analysis, Writing - original draft. **Luis Javier Sánchez-Aparicio:** Conceptualization, Methodology, Writing - review & editing. **José G. Fueyo:** Software, Writing - review & editing. **Javier Pisonero:** Formal analysis, Visualization. **Diego González-Aguilera:** Supervision, Writing - review & editing.

Declaration of Competing Interest

The authors declare that they have no known competing financial interests or personal relationships that could have appeared to influence the work reported in this paper.

Acknowledgements

This work was financed by ERDF funds through the V Sudoe Interreg program within the framework of the COMPRESSer project, Ref. SOE2/P1/E0643. Thanks also to the support provided by the Ministry of Science, Innovation and Universities through the project FaTIMA, Ref. RTI2018-099850-B-I00.

References

[1] G. Sinclair, J. Helms, A review of simple formulae for elastic hoop stresses in cylindrical and spherical pressure vessels: what can be used when, Int. J. Press. Vessels Pip. 128 (2015) 1–7.
[2] N. Yahaya, N.M. Noor, S.R. Othman, L.K. Sing, M.M. Din, New technique for studying soil-corrosion of underground pipeline, J. Appl. Sci. 11 (2011) 1510–1518.
[3] G.H. Koch, M.P. Brongers, N.G. Thompson, Y.P. Virmani, J.H. Payer, Corrosion Cost and Preventive Strategies in the United States, Federal Highway Administration, United States, 2002.
[4] D.D.N. Veritas, DNV-OS-C501–Composite Components–Offshore Standard, 2003.
[5] M. Mokhtari, A.A. Nia, The application of CFRP to strengthen buried steel pipelines against subsurface explosion, Soil Dyn. Earthq. Eng. 87 (2016) 52–62.
[6] M.F. Ashby, Chapter 5 – Materials Selection. Materials Selection in Mechanical Design cop (2011.) 97–124.
[7] R. Rafiee, On the mechanical performance of glass-fibre-reinforced thermosetting-resin pipes: a review, Compos. Struct. 143 (2016) 151–164.
[8] P. Laney, Use of Composite Pipe Materials in the Transportation of Natural Gas, Idaho International Engineering and Environmental Laboratory, Bechtel BWXT Idaho, LLC, 2002.
[9] R. Rafiee, B. Mazhari, Evaluating long-term performance of Glass Fiber Reinforced Plastic pipes subjected to internal pressure, Constr. Build. Mater. 122 (2016) 694–701.
[10] R. Rafiee, B. Mazhari, Simulation of the long-term hydrostatic tests on glass fiber reinforced plastic pipes, Compos. Struct. 136 (2016) 56–63.
[11] R. Rafiee, F. Elasmi, Theoretical modeling of fatigue phenomenon in composite pipes, Compos. Struct. 161 (2017) 256–263.
[12] J.C. Velosa, J.P. Nunes, P. Antunes, J. Silva, A. Marques, Development of a new generation of filament wound composite pressure cylinders, Compos. Sci. Technol. 69 (2009) 1348–1353.
[13] A. Zaman, S.A. Gutub, M.A. Wafa, A review on FRP composites applications and durability concerns in the construction sector, J. Reinf. Plast. Compos. 32 (2013) 1966–1988.
[14] C. Colombo, L. Vergani, Optimization of filament winding parameters for the design of a composite pipe, Compos. B Eng. 148 (2018) 207–216.

[15] R. Rafiee, M.A. Torabi, S. Maleki, Investigating structural failure of a filament-wound composite tube subjected to internal pressure: experimental and theoretical evaluation, Polym. Test. 67 (2018) 322–330.
[16] K.S. Lim, S. Azraai, N. Noor, N. Yahaya, An overview of corroded pipe repair techniques using composite materials, Int. J. Mater. Metall. Eng. 10 (2016) 19–25.
[17] E. Mahdi, E. Eltai, Development of cost-effective composite repair system for oil/gas pipelines, Compos. Struct. 202 (2018) 802–806.
[18] M. Kara, M. Uyaner, A. Avci, Repairing impact damaged fiber reinforced composite pipes by external wrapping with composite patches, Compos. Struct. 123 (2015) 1–8.
[19] R. Rafiee, M. Fakoor, H. Hesamsadat, The influence of production inconsistencies on the functional failure of GRP pipes, Steel Compos. Struct. 19 (2015) 1369–1379.
[20] J.N. Reddy, Mechanics of Laminated Composite Plates and Shells: Theory and Analysis, CRC Press, 2003.
[21] S. Sriramula, M.K. Chryssanthopoulos, Quantification of uncertainty modelling in stochastic analysis of FRP composites, Compos. A Appl. Sci. Manuf. 40 (2009) 1673–1684.
[22] O. Orell, J. Vuorinen, J. Jokinen, H. Kettunen, P. Hytönen, J. Turunen, et al., Characterization of elastic constants of anisotropic composites in compression using digital image correlation, Compos. Struct. 185 (2018) 176–185.
[23] S. Sharifi, S. Gohari, M. Sharifiteshnizi, R. Alebrahim, C. Burvill, Y. Yahya, et al., Fracture of laminated woven GFRP composite pressure vessels under combined low-velocity impact and internal pressure, Arch. Civil Mech. Eng. 18 (2018) 1715–1728.
[24] M. Tekieli, S. De Santis, G. de Felice, A. Kwiecień, F. Roscini, Application of Digital Image Correlation to composite reinforcements testing, Compos. Struct. 160 (2017) 670–688.
[25] M.A. Seif, U.A. Khashaba, R. Rojas-Oviedo, Measuring delamination in carbon/epoxy composites using a shadow moiré laser based imaging technique, Compos. Struct. 79 (2007) 113–118.
[26] P. Callaway, M. Gilbert, C.C. Smith, Influence of backfill on the capacity of masonry arch bridges, in: Proceedings of the Institution of Civil Engineers: Bridge Engineering, ICE Publishing, 2012, pp. 147–157.
[27] L. Sánchez-Aparicio, A. Villarino, J. García-Gago, D. González-Aguilera, Photogrammetric, geometrical, and numerical strategies to evaluate initial and current conditions in historical constructions: a test case in the church of San Lorenzo (Zamora, Spain), Remote Sens. 8 (2016) 60.
[28] B. Pan, Digital image correlation for surface deformation measurement: historical developments, recent advances and future goals, Meas. Sci. Technol. 29 (2018) 082001.
[29] S.M. Daghash, O.E. Ozbulut, Flexural performance evaluation of NSM basalt FRP-strengthened concrete beams using digital image correlation system, Compos. Struct. 176 (2017) 748–756.
[30] C. Unlusoy, G.W. Melenka, Flexural testing of cellulose fiber braided composites using three dimensional digital image correlation, Compos. Struct. 230 (2019) 111538.
[31] T. He, L. Liu, A. Makeev, Uncertainty analysis in composite material properties characterization using digital image correlation and finite element model updating, Compos. Struct. 184 (2018) 337–351.
[32] L. Yu, B. Pan, Experimental study of tensile properties and deformation evolutions of 2D and 2.5 D woven SiO2f/SiO2 composites using single-camera stereo-digital image correlation, Compos. Struct. 200 (2018) 589–598.
[33] P. Kowalczyk, Identification of mechanical parameters of composites in tensile tests using mixed numerical-experimental method, Measurement 135 (2019) 131–137.
[34] J. Ahn, E. He, L. Chen, J. Dear, Z. Shao, C. Davies, In-situ micro-tensile testing of AA2024-T3 fibre laser welds with digital image correlation as a function of welding speed, Int. J. Lightweight Mater. Manuf. 1 (2018) 179–188.
[35] D. Xu, C. Cerbu, H. Wang, I.C. Rosca, Analysis of the hybrid composite materials reinforced with natural fibers considering digital image correlation (DIC) measurements, Mech. Mater. 135 (2019) 46–56.
[36] R. Garcia-Martin, Á. Bautista-De Castro, L.J. Sánchez-Aparicio, J.G. Fueyo, D. Gonzalez-Aguilera, Combining digital image correlation and probabilistic approaches for the reliability analysis of composite pressure vessels, Arch. Civil Mech. Eng. 19 (2019) 224–239.
[37] G. das Neves Carneiro, CC. António, Global optimal reliability index of implicit composite laminate structures by evolutionary algorithms, Struct. Saf. 79 (2019) 54–65.
[38] R. Rafiee, M.A. Torabi, Stochastic prediction of burst pressure in composite pressure vessels, Compos. Struct. 185 (2018) 573–583.
[39] R. Rafiee, F. Reshadi, S. Eidi, Stochastic analysis of functional failure pressures in glass fiber reinforced polyester pipes, Mater. Des. 67 (2015) 422–427.
[40] R. Rafiee, Stochastic fatigue analysis of glass fiber reinforced polymer pipes, Compos. Struct. 167 (2017) 96–102.
[41] S.S. Tomar, S. Zafar, M. Talha, W. Gao, D. Hui, State of the art of composite structures in non-deterministic framework: a review, Thin-Walled Struct. 132 (2018) 700–716.
[42] S. Dey, T. Mukhopadhyay, S. Adhikari, Metamodel based high-fidelity stochastic analysis of composite laminates: a concise review with critical comparative assessment, Compos. Struct. 171 (2017) 227–250.
[43] ISO E, Plastics–determination of tensile properties, 1997.
[44] H. Toutanji, S. Dempsey, Stress modeling of pipelines strengthened with advanced composites materials, Thin-Walled Struct. 39 (2001) 153–165.
[45] ISO E. 527-4, Plastics–determination of tensile properties–part 4: test conditions for isotropic and orthotropic fibre-reinforced plastic composites, International Organization for Standardization (ISO), Geneva, Switzerland, 1997.
[46] M.A. Sutton, J.J. Orteu, H. Schreier, Image Correlation for Shape, Motion and Deformation Measurements: Basic Concepts, Theory and Applications, Springer Science & Business Media, 2009.
[47] B. Pan, K. Qian, H. Xie, A. Asundi, Two-dimensional digital image correlation for in-plane displacement and strain measurement: a review, Meas. Sci. Technol. 20 (2009) 062001.
[48] Y. Dong, B. Pan, A review of speckle pattern fabrication and assessment for digital image correlation, Exp. Mech. 57 (2017) 1161–1181.
[49] M.N. Vo, Z. Wang, L. Luu, J. Ma, Advanced geometric camera calibration for machine vision, Opt. Eng. 50 (2011) 110503.
[50] L.A. Martins, F.L. Bastian, T.A. Netto, Structural and functional failure pressure of filament wound composite tubes, Mater. Design (1980-2015) 36 (2012) 779–787.
[51] S.W. Tsai, E.M. Wu, A general theory of strength for anisotropic materials, J. Compos. Mater. 5 (1971) 58–80.
[52] L. Novak, D. Novak, Polynomial chaos expansion for surrogate modelling: theory and software, Beton-und Stahlbetonbau 113 (2018) 27–32.
[53] Á. Bautista-De Castro, L.J. Sánchez-Aparicio, P. Carrasco-García, L.F. Ramos, D. González-Aguilera, A multidisciplinary approach to calibrating advanced numerical simulations of masonry arch bridges, Mech. Syst. Sig. Process. 129 (2019) 337–365.
[54] N. Wiener, The homogeneous chaos, Am. J. Math. 60 (1938) 897–936.
[55] G. Blatman, B. Sudret, Adaptive sparse polynomial chaos expansion based on least angle regression, J. Comput. Phys. 230 (2011) 2345–2367.
[56] B. Efron, T. Hastie, I. Johnstone, R. Tibshirani, Least angle regression, Ann. Stat. 32 (2004) 407–499.
[57] G. Deman, K. Konakli, B. Sudret, J. Kerrou, P. Perrochet, H. Benabderrahmane, Using sparse polynomial chaos expansions for the global sensitivity analysis of groundwater lifetime expectancy in a multi-layered hydrogeological model, Reliab. Eng. Syst. Saf. 147 (2016) 156–169.
[58] D. Lecompte, H. Sol, J. Vantomme, A. Habraken, Analysis of speckle patterns for deformation measurements by digital image correlation, Int. Soc. Opt. Photon. (2006) 63410E.
[59] B. Pan, Z. Lu, H. Xie, Mean intensity gradient: an effective global parameter for quality assessment of the speckle patterns used in digital image correlation, Opt. Lasers Eng. 48 (2010) 469–477.
[60] A.F. Ab Ghani, M.B. Ali, S. DharMalingam, J. Mahmud, Digital image correlation (DIC) technique in measuring strain using opensource platform Ncorr, J. Adv. Res. Appl. Mech. 26 (2016) 10–21.
[61] P. Sasikumar, R. Suresh, P.K. Vijayaghosh, S. Gupta, Experimental characterisation of random field models for CFRP composite panels, Compos. Struct. 120 (2015) 451–471.
[62] R.B. D'Agostino, Goodness-of-fit-techniques, CRC press, 1986.
[63] H. Liu, Pipeline Engineering, CRC Press, 2003.
[64] S. Marelli, B. Sudret, UQLab: A framework for uncertainty quantification in Matlab. Vulnerability, Uncertainty, and Risk: Quantification, Mitigation, and Management (2014) 2554 2563
[65] M.D. McKay, R.J. Beckman, W.J. Conover, Comparison of three methods for selecting values of input variables in the analysis of output from a computer code, Technometrics 21 (1979) 239–245.
[66] D. Goldberg, Genetic Algorithms in Search, Optimization & Machine Learning, Addison-Wesley Publishing Company, Inc., 1989.
[67] M. Mitchell, An Introduction to Genetic Algorithms, MIT Press, 1998.